

Anisotropic Skyrmion and Multi- q Spin Dynamics in Centrosymmetric Gd_2PdSi_3

M. Gomilšek,^{1,2,3,*} T. J. Hicken,^{4,3} M. N. Wilson,^{5,3} K. J. A. Franke,^{6,3} B. M. Huddart,^{7,3} A. Štefančič,⁸ S. J. R. Holt,^{8,†} G. Balakrishnan,⁸ D. A. Mayoh,⁸ M. T. Birch,^{9,10,3} S. H. Moody,^{11,3} H. Luetkens,⁴ Z. Guguchia,⁴ M. T. F. Telling,¹² P. J. Baker,¹² S. J. Clark,³ and T. Lancaster³

¹*Jožef Stefan Institute, Jamova c. 39, SI-1000 Ljubljana, Slovenia*

²*Faculty of Mathematics and Physics, University of Ljubljana, Jadranska u. 19, SI-1000 Ljubljana, Slovenia*

³*Department of Physics, Durham University, South Road, Durham DH1 3LE, United Kingdom*

⁴*Laboratory for Muon Spin Spectroscopy, Paul Scherrer Institut, 5232 Villigen PSI, Switzerland*

⁵*Department of Physics and Physical Oceanography, Memorial University, A1B 3X7, Canada*

⁶*School of Physics and Astronomy, University of Leeds, LS2 9JT, United Kingdom*

⁷*Clarendon Laboratory, University of Oxford, Department of Physics, Oxford OX1 3PU, United Kingdom*

⁸*University of Warwick, Department of Physics, Coventry CV4 7AL, United Kingdom*

⁹*Max Planck Institute for Intelligent Systems, Heisenbergstrasse 3, D-70569 Stuttgart, Germany*

¹⁰*RIKEN Center for Emergent Matter Science, JP-351-0198 Wako, Japan*

¹¹*Laboratory for Neutron Scattering and Imaging,*

Paul Scherrer Institut, 5232 Villigen PSI, Switzerland

¹²*ISIS Facility, STFC Rutherford Appleton Laboratory,*

Didcot, Oxfordshire OX11 0QX, United Kingdom

(Dated: March 14, 2024)

Skyrmions are particle-like vortices of magnetization with non-trivial topology, which are usually stabilized by Dzyaloshinskii–Moriya interactions (DMI) in noncentrosymmetric bulk materials. Exceptions are centrosymmetric Gd- and Eu-based skyrmion-lattice (SkL) hosts with net-zero DMI, where both the SkL stabilization mechanisms and magnetic ground states remain controversial. We address these by investigating both static and dynamic spin properties of the centrosymmetric SkL host Gd_2PdSi_3 using muon spectroscopy (μSR). We find that spin fluctuations in its non-coplanar SkL phase are highly anisotropic, implying that spin anisotropy plays a prominent role in stabilizing this phase. We also observe strongly-anisotropic spin dynamics in the ground-state (IC-1) incommensurate magnetic phase of the material, indicating that it is a meron-like multi- q structure. In contrast, the higher-field, coplanar IC-2 phase is found to be single- q with nearly-isotropic spin dynamics.

Topological spin textures can support exotic spin dynamics with a range of potential applications [1, 2]. Especially promising are materials hosting skyrmions, which are topologically-protected, non-coplanar magnetization vortices that behave as extended particles [1, 3]. Usually found in bulk noncentrosymmetric materials and stabilized by Dzyaloshinskii–Moriya interactions (DMI), which select a skyrmion helicity [4], they were also found to be stabilized by competing magnetic interactions in bulk centrosymmetric compounds with no preferred helicity and no net DMI [1, 2]. Examples are Gd_2PdSi_3 , with a triangular spin lattice [5–11], $\text{Gd}_3\text{Ru}_4\text{Al}_{12}$ with a breathing kagome spin lattice [11–14], and GdRu_2Si_2 [15–20], GdRu_2Ge_2 [21], and EuAl_4 [22–24] with tetragonal spin lattices. Common to these highly-symmetric rare-earth materials is that they host incommensurate skyrmion-lattice (SkL) phases with very small (1.9–3.5 nm) skyrmions that are stable under higher applied fields (~ 1 T) and over a wider range of T than their DMI-stabilized counterparts [1, 2].

The stabilization mechanism for centrosymmetric skyrmions is controversial, with suggestions including: (i) short-range geometrical frustration [13, 25–28], (ii) long-range Ruderman–Kittel–Kasuya–Yosida (RKKY) plus dipolar [18, 20, 29, 30] or biquadratic exchange inter-

actions [17, 21, 31–35], and (iii) competition of orbital-dependent exchange [36, 37]. Most, but not all [31, 32], scenarios require spin anisotropy. Furthermore, the zero-field (ZF) ground state is also contentious [10], with early studies of Gd_2PdSi_3 suggesting an exotic, triple- q magnetic structure [5, 6] (e.g., a lattice of merons and antimerons, which are half-skyrmion-like spin textures [17, 21]), while recent calculations under scenario (ii) indicated a simpler, single- q helical ground state [29], as in DMI-stabilized SkL hosts [38]. Investigations of centrosymmetric SkL hosts have mostly focused on their static and topological properties, with less attention [24] paid to emergent spin dynamics [26], which can elucidate both the stabilization mechanism and single- or multi- q nature. In contrast, characteristic dynamics of SkL and related spin textures have been observed in a range of DMI-stabilized SkL hosts [1, 2, 39–41]. For accessing these, muon spectroscopy (μSR), a local-probe technique sensitive to spin fluctuations over a unique frequency range [42], has proven valuable [43–49]. However, the narrow T range of DMI skyrmions [1, 2, 38] limited the ability to extract the underlying spin-wave dispersions.

In this Letter we investigate the most-studied centrosymmetric SkL host Gd_2PdSi_3 [5] using μSR and AC susceptibility, complemented by density functional the-

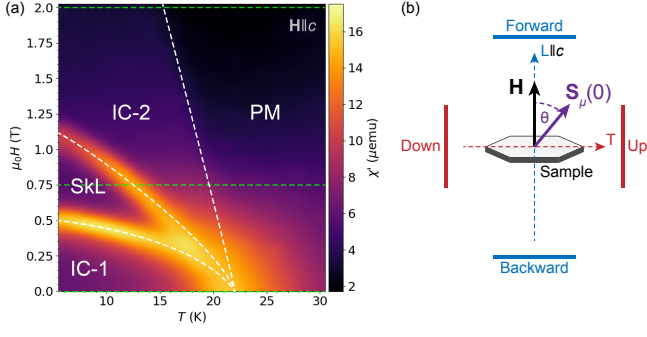


Fig. 1. (a) Real part of AC susceptibility with applied field along the crystallographic c axis. Phase boundaries (white) and μ SR scans (green) are shown. (b) Sample and detector arrangement for μ SR measurements. The initial muon spin $\mathbf{S}_\mu(0)$ lies at an angle θ to the applied field $\mathbf{H} \parallel c$, which points along the longitudinal direction L (blue). The transverse direction T (red) lies in the hexagonal ab plane.

ory (DFT) calculations of muon stopping sites [50]. We find clear signatures of spin reorientation transitions between the incommensurate magnetic phases and reveal the highly anisotropic character of their spin fluctuations. By exploiting the wide T stability of these phases, we characterize the low-energy dispersion relations of their spin-wave excitations. In the higher-field coplanar incommensurate IC-2 phase these are consistent with a single- q fan-like spin texture [5, 6] with nearly-isotropic spin fluctuations. However, in the ground-state ZF incommensurate IC-1 phase in-plane (ab -plane), we find that low-energy spin fluctuations dominate while out-of-plane (c -axis) spin fluctuations are almost completely suppressed. This indicates that the IC-1 phase is a complex, triple- q magnetic structure [5, 6], not the recently-predicted single- q helical structure [29], disfavoring SkL-stabilization scenario (ii) described above. Finally, in the SkL phase out-of-plane fluctuations dominate instead, with in-plane fluctuations suppressed as a power-law in T . We therefore argue that spin anisotropy is a key ingredient in stabilizing the SkL phase in centrosymmetric rare-earth magnets.

Single crystals of Gd_2PdSi_3 were synthesized, with five high-quality $\approx 9 \text{ mm}^2 \times 0.6 \text{ mm}$ plate-like crystallites with c -axis normals extracted [50]. AC magnetic susceptibility measurements reproduced the phase diagram from previous studies [5–7], including the SkL phase [Fig. 1(a)]. For μ SR measurements, the crystallites were assembled in a mosaic with coaligned c axes [50]. The initial muon spin orientation pointed along the normal (c -axis) direction in longitudinal-field (LF) measurements ($\theta = 0$), and at an angle of $\theta \approx 50^\circ$ away from the c axis in ZF and transverse-field (TF) measurements [Fig. 1(b)]. In ZF and TF, both the longitudinal- ($L \parallel c$) and transverse- ($T \perp c$) muon spin component could thus be measured separately, while in LF the L muon spin component was

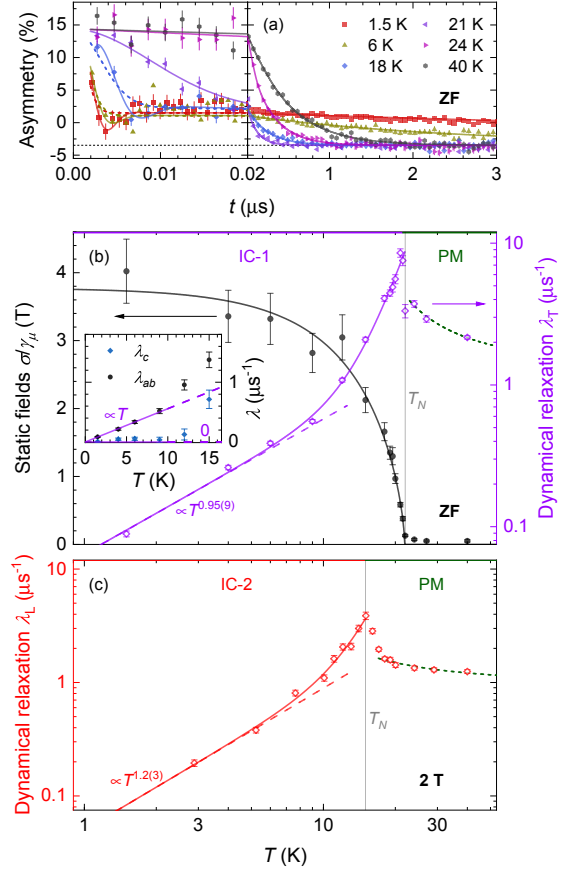


Fig. 2. (a) T-direction muon asymmetry at early (left) and late times (right) in the IC-1 phase in ZF. Solid lines on the left panel are guides to the eye; dashed lines are fits using the model described in the text. (b) In-plane quasi-static magnetic fields (black) and dynamic relaxation rates (violet) in the IC-1 phase in ZF. Inset: contributions to relaxation due to out-of-plane (c -axis, blue) and in-plane (ab -plane, black) spin fluctuations. (c) Relaxation due to in-plane fluctuations in the IC-2 phase in a 2 T field. Solid lines over $\lambda_{T,L}$ in (b,c) at $T < T_N$ are guides to the eye (sum of two power laws); dashed lines are the single-power-law low- T limits.

measured. All measurements were made after first zero field cooling (ZFC) the sample to base T , while magnetic fields were always applied along the out-of-plane (c -axis) direction, which is an axis of threefold crystallographic symmetry and thus a magnetic eigenaxis.

We first performed μ SR measurements on warming from the IC-1 ground-state of Gd_2PdSi_3 in ZF on the GPS instrument at the Swiss Muon Source ($S\mu S$). At low T , a highly-damped oscillation in the T-muon-spin component was observed at early times $t \ll 0.1 \mu\text{s}$ [Fig. 2(a)] due to a broad distribution of quasi-static local fields at the muon site, which originate from long-range incommensurate magnetic ordering of Gd^{3+} spins. At late times, up to $t \approx 10 \mu\text{s}$, a further exponential relaxation was observed due to dynamic fluctuations of Gd^{3+} spins slower than the muon precession frequency [42] (faster

fluctuations would have wiped out early-time oscillations). A damped oscillation model proved unreliable in fits [50]. The measured T muon asymmetry data were thus fit using $A(t) = [a_s - a_r]e^{-\sigma^2 t^2} + a_r e^{-\lambda t} + a_{\text{bgd}}$, where $a_s = \text{const.}$ is the total sample asymmetry, the early-time relaxation rate σ is proportional to the width of the quasi-static local-magnetic-field distribution (and thus to the average magnitude of internal fields), a_r is the late-time relaxing asymmetry due to the fraction of local fields that initially point along the measured muon spin component, λ is the late-time dynamic relaxation rate due to slow fluctuations of fields orthogonal to the measured muon-spin component [42, 50], and $a_{\text{bgd}} = \text{const.}$ is the background due to muons hitting the sample holder.

Fit results for the T direction are shown in Fig. 2(b) with the transition temperature $T_N = 22(1)$ K consistent with AC susceptibility [Fig. 1(a)]. In the itinerant paramagnetic (PM) regime at $T > T_N$ there are no average quasi-static fields ($\sigma \approx 0$). Around $T \approx T_N$ spin fluctuations exhibit a critical divergence characteristic of a continuous phase transition as we enter the IC-1 phase. Finally, in the IC-1 phase at $T < T_N$ the local field strength increases and saturates as an order parameter, $\sigma \propto [1 - (T/T_N)^{3/2}]^\beta$ [24, 42] with $\beta = 0.7(1)$, which is large but close to $\beta = 0.50(5)$ found in the centrosymmetric SkL host EuAl_4 in ZF [24], while slow spin fluctuations cross over into a low- T power-law $\lambda_T \propto T^p$ with $p = 0.95(9)$. A low- T power-law dependence of the dynamic relaxation rate could be understood within spin-wave theory for a two-magnon process, which for a single gapless magnon band predicts [50–52]

$$p = \frac{2D}{s} - 1, \quad (1)$$

where D is the dimensionality of spin-wave excitations and s is the dominant power in their dispersion relation $\omega \propto |\mathbf{q} - \mathbf{q}_0|^s$ around the ordering wave vector \mathbf{q}_0 . Usually, $s = 2$ for ferromagnetic ($\mathbf{q}_0 = 0$) and $s = 1$ for antiferromagnetic and incommensurate states ($\mathbf{q}_0 \neq 0$) [53]. The measured T-direction $p \approx 1$ in IC-1 phase would thus correspond to a 1D (single- q) magnetic structure ($D = s = 1$), if the single-band approximation were valid.

To test this scenario, we also fitted the L-direction ZF μSR data using the same model to obtain the relaxation rate λ_L . Assuming bulk uniaxial symmetry, with a magnetic eigenaxis c and eigenplane ab , we can further write [42, 50]: $\lambda_L = 2\lambda_{ab}$ and $\lambda_T = \lambda_{ab} + \lambda_c$, where λ_{ab} and λ_c are the contributions to the muon relaxation rate due to dynamic fluctuations of in-plane and out-of-plane magnetic fields at the muon site, respectively. At the nearly-symmetric in-plane muon site we obtain from DFT calculations, λ_{ab} and λ_c arise from dynamics of in-plane and out-of-plane Gd^{3+} spin components, respectively [50], especially if interlayer correlations are ferromagnetic, as found in Refs. [29, 30]. Inset in Fig. 2(b) shows the extracted in-plane λ_{ab} and out-of-plane λ_c [50].

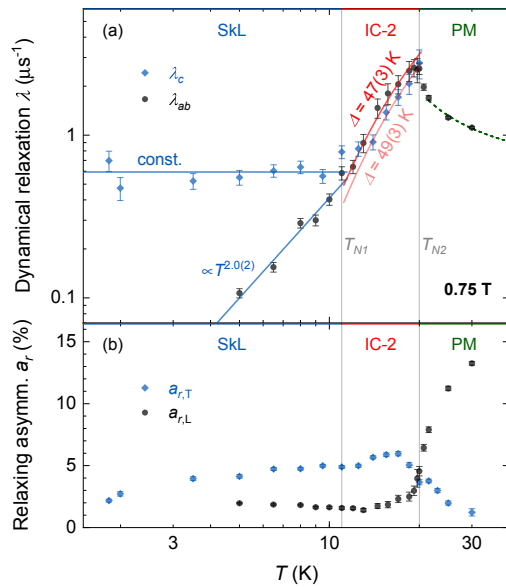


Fig. 3. (a) Relaxation rates due to out-of-plane (c -axis, blue) and in-plane (ab -plane, black) spin fluctuations in the SkL and IC-2 phases in a 0.75 T applied field. (b) Relaxing asymmetry due to quasi-static local fields within the ab plane (blue) and along the c axis (black) under the same conditions.

Remarkably, in contrast to the single-magnon-band approximation, where we should have $\lambda_{ab} \propto \lambda_c \propto T^p$, we instead find $\lambda_{ab} \propto T$ but $\lambda_c \approx 0 \ll \lambda_{ab}$ in the IC-1 phase. Our first result is therefore that the IC-1 phase is not a simple single- q magnetic structure as was recently predicted [29]. Instead, there appear to be multiple, highly-anisotropic spin-fluctuation modes in the IC-1 phase, as expected, e.g., for extended, multi- q spin textures [26, 39], such as the hypothesized meron–antimeron lattice state [5, 6]. Their predominantly in-plane nature appears consistent with easy-plane anisotropy found in this phase [10].

Next, we turn to the IC-2 and SkL phases. Here we performed separate μSR measurements in a TF of 0.75 T on the GPS instrument at $\text{S}\mu\text{S}$ and a LF of 0.75 T on the HiFi instrument at the STFC-ISIS Facility. The advantage of the latter were higher statistics at late times, though with lower temporal resolution. We warmed from the low- T SkL to the intermediate IC-2 and finally to the PM phase [Fig. 1(a)]. The late-time data were well described by the same model as for the ZF data, simplifying to $A(t) = a_r e^{-\lambda t} + a_{\text{bgd}}$ at late times. From T-direction TF data and L-direction LF data we extracted in-plane λ_{ab} and out-of-plane λ_c spin-fluctuation contributions to muon relaxation via the relations described above [50].

The relaxation rates are shown in Fig. 3(a) with transition temperatures $T_{N1} = 11(1)$ K and $T_{N2} = 20(1)$ K consistent with AC susceptibility [Fig. 1(a)]. The in-plane relaxation rate λ_{ab} shows a critical divergence at $T \approx T_{N2}$ due to a continuous transition between the PM

and IC-2 phases. In the IC-2 regime at $T_{N1} < T < T_{N2}$ we find nearly-isotropic spin fluctuations with $\lambda_c \approx \lambda_{ab}$; fitted to an empirical gapped model $\propto e^{-\Delta/T}$, λ_c and λ_{ab} also yield the same characteristic energy scales $\Delta = 47(3)$ and $49(3)$ K, respectively. However, any low- T power-law spin-wave behaviour [Eq. (1)] is masked by near-critical fluctuations and interrupted by a transition to the SkL phase at T_{N1} . This phase transition does not show any critical divergence in the muon relaxation rate, only a change of slope, implying that it is first-order, consistent with the topologically-non-trivial nature of the SkL [1, 26]. Similarly to the IC-1 phase, we find that highly anisotropic spin fluctuations appear with lowering $T < T_{N1}$. Intriguingly, while in the IC-1 phase spin fluctuations were predominantly in-plane, $\lambda_c \ll \lambda_{ab}$, the dominant spin fluctuations in the SkL phase are instead out-of-plane, $\lambda_c \approx \text{const.} \gg \lambda_{ab} \propto T^p$ with $p = 2.0(2)$. We note that $p \approx 2$ would correspond to $D = 3$, $s = 2$ (3D ferromagnetic) spin excitations in the single-band spin-wave approximation [Eq. (1)], but this is inconsistent with a T -independent λ_c . Instead, there appears to be a large low-energy spin density of states due to multiple spin fluctuation modes, as expected for SkL phases [26, 39–41, 54], that are predominantly polarized out-of-plane (e.g., skyrmion breathing modes [39, 54]).

We next turn to quasi-static SkL and IC-2 signatures under 0.75 T. Fig. 3(b) shows late-time relaxing asymmetries $a_{r,T}$ and $a_{r,L}$ in the T (in-plane) and L (out-of-plane) directions, respectively [Fig. 1(b)]. Both change rather abruptly at $T \approx T_{N2}$ due to the onset of magnetic order. Assuming bulk uniaxial symmetry, with a magnetic eigenaxis c and eigenplane ab , we have, in ordered magnetic phases [42, 50]: $a_{r,T} = a_{s,T} \langle \hat{B}_a^2 \rangle$ and $a_{r,L} = a_{s,L} \langle \hat{B}_c^2 \rangle$, where $\hat{\mathbf{B}} = \mathbf{B}/|\mathbf{B}|$ is the initial local-field direction, $a_{s,T}$ and $a_{s,L}$ are the total sample asymmetries along the T and L detector directions, and $\langle \dots \rangle$ denotes an ensemble average over the muons. In Fig. 3(b) we see that $a_{r,T} \propto \langle \hat{B}_a^2 \rangle = \langle \hat{B}_b^2 \rangle$ exhibits a broad peak in the IC-2 phase at $T_{N1} < T < T_{N2}$, while $a_{r,L} \propto \langle \hat{B}_c^2 \rangle = 1 - 2 \langle \hat{B}_a^2 \rangle$ exhibits a minimum, both indicating mainly coplanar quasi-static magnetism in this phase. On the other hand, the difference between $a_{r,T}$ and $a_{r,L}$ becomes smaller in the SkL phase, implying that local field directions become more isotropic, as expected for non-coplanar spin textures [1–3]. The observed coplanar nature of the IC-2 phase and non-coplanar nature of the SkL phase is consistent with resonant X-ray scattering (RXS) results of Ref. [5], where this was argued based on the ellipticity (m_c/m_{ab}) of magnetic moments $\mathbf{m}(\mathbf{q})$ of individual magnetic Bragg peaks in \mathbf{q} -space. However, our conclusions are based on a complementary [10], real-space determination of local field directions only accessible to local probes like the muon [42].

Finally, to assess the low- T dynamics of the IC-2 phase we performed μ SR measurements in a LF of 2 T on the HiFi instrument. The late-time L-direction muon data

were well described by the same model as for the 0.75 T data, where the fitted relaxation rate $\lambda_L = 2\lambda_{ab}$ [see Fig. 2(c)] shows a transition temperature $T_N = 15(1)$ K consistent with AC susceptibility [Fig. 1(a)]. Near $T \approx T_N$ the muon relaxation rate exhibits a critical divergence characteristic of a continuous phase transition as we enter the IC-2 phase, and at $T < T_N$ it crosses over into a low- T power-law $\lambda_L \propto T^p$ with $p = 1.2(3)$. The observed isotropy of spin fluctuations in this phase [Fig. 3(a)] makes single-band spin-wave theory [Eq. (1)] applicable, with the measured $p \approx 1$ indicating that the IC-2 phase is a 1D (single- q) magnetic structure ($D = s = 1$), as previously suggested [5, 6]. This stands in contrast to multi- q IC-1 and SkL phases found at lower applied fields.

Our finding of fundamentally different low- T in-plane and out-of-plane spin fluctuations in both non-coplanar, SkL and ground-state IC-1, phases of centrosymmetric Gd_2PdSi_3 contrasts with isotropic fluctuations found in the coplanar single- q IC-2 phase. This should be a clue to the stabilization mechanism for centrosymmetric skyrmions. However, in contrast to DMI-stabilized skyrmions, where their dynamics were studied [39–41, 54, 55], systematic predictions for SkL spin dynamics under different stabilization-mechanism scenarios are lacking. Nevertheless, it seems unlikely that a spin model without strong intrinsic anisotropy could explain the observed, highly-anisotropic SkL and IC-1 spin dynamics. This agrees with suggestions that spin anisotropy [10, 26, 35], combined with long-range interactions, should be important for stabilizing the SkL phase [30, 33]. Furthermore, our observation that the ground-state IC-1 phase is a triple- q magnetic structure suggests it is likely the exotic meron-antimeron lattice state, as hypothesized in Ref. [5] based on RXS and field-dependent Hall resistivity measurements. This result represents another challenge to theory, as recent calculations suggested that this phase should instead be single- q under the RKKY+dipolar skyrmion stabilization scenario (ii) [30]. Our findings thus disfavour this scenario as the dominant skyrmion stabilization mechanism. Nevertheless, RKKY interactions were found to be strong in the related centrosymmetric SkL host GdRu_2Si_2 via angle-resolved photoemission spectroscopy (ARPES) [20] and quantum-oscillation measurements [18], complemented by *ab initio* calculations [17, 18, 20], so they could still play a role.

In conclusion, in our local-probe study of centrosymmetric Gd_2PdSi_3 we have found large anisotropy of spin dynamics, with qualitatively different behaviour of dominant out-of-plane and subdominant in-plane spin fluctuations in its SkL phase. We have established the meron-like triple- q nature of its incommensurate IC-1 ground state with dominant in-plane, and nearly-absent out-of-plane, fluctuations. The higher-field IC-2 phase was found to be coplanar and single- q with isotropic spin fluctuations. Our results suggest that the enigmatic stabilization mechanism behind SkL phases in centrosym-

metric Gd- and Eu-based materials is likely to be intimately related to strong spin anisotropy, and not solely RKKY+dipolar. Further local-probe studies of these and related centrosymmetric compounds [1, 2, 56, 57] should be informative in exploring this. Our methods could also be extended to study low- T spin anisotropy and dynamics of metastable skyrmions in DMI-based SkL hosts [1].

Research data presented in this paper will be made available on the figshare repository at doi:XXXX.

We thank Martin Klanjšek and Matej Pregelj at the Jožef Stefan Institute, Slovenia for helpful discussions. Parts of the work were carried out at the STFC ISIS Muon Source, United Kingdom and at the Swiss Muon Source, Paul Scherrer Institute, Switzerland and we are grateful for the provision of beamtime and experimental support. We thank Raymond Fan and Paul Steadman for enabling us to use the Quantum Design MPMS3 at the I10 support laboratory, Diamond Light Source for AC susceptibility measurements. Computing resources were provided by the Durham HPC Hamilton cluster. M.G. acknowledges the financial support of the Slovenian Research and Innovation Agency through Program No. P1-0125 and Projects No. Z1-1852, N1-0148, J1-2461, J1-50008, and J1-50012. We acknowledge the financial support of the Engineering and Physical Sciences Research Council (EPSRC, UK) through Grants No. EP/N032128/1 and EP/N024028/1. The work at the University of Warwick was also funded by EPSRC, UK through Grant No. EP/T005963/1.

* matjaz.gomilsek@ijs.si

† Current addresses: Faculty of Engineering and Physical Sciences, University of Southampton, Southampton SO17 1BJ, United Kingdom; Max Planck Institute for the Structure and Dynamics of Matter, Luruper Chaussee 149, 22761 Hamburg, Germany

- [1] S. Li, X. Wang, and T. Rasing, Magnetic skyrmions: Basic properties and potential applications, *Interdiscip. Mater.* **2**, 260 (2023).
- [2] J. Khatua, B. Sana, A. Zorko, M. Gomilšek, K. Sethupathi, M. R. Rao, M. Baenitz, B. Schmidt, and P. Khuntia, Experimental signatures of quantum and topological states in frustrated magnetism, *Phys. Rep.* **1041**, 1 (2023).
- [3] T. Lancaster, Skyrmions in magnetic materials, *Contemp. Phys.* **60**, 246 (2019).
- [4] D. Morikawa, K. Shibata, N. Kanazawa, X. Z. Yu, and Y. Tokura, Crystal chirality and skyrmion helicity in MnSi and (Fe, Co)Si as determined by transmission electron microscopy, *Phys. Rev. B* **88**, 024408 (2013).
- [5] T. Kurumaji, T. Nakajima, M. Hirschberger, A. Kikkawa, Y. Yamasaki, H. Sagayama, H. Nakao, Y. Taguchi, T. H. Arima, and Y. Tokura, Skyrmion lattice with a giant topological hall effect in a frustrated triangular-lattice magnet, *Science* **365**, 914 (2019).
- [6] M. Hirschberger, T. Nakajima, M. Kriener, T. Kurumaji, L. Spitz, S. Gao, A. Kikkawa, Y. Yamasaki, H. Sagayama, H. Nakao, S. Ohira-Kawamura, Y. Taguchi, T. H. Arima, and Y. Tokura, High-field depinned phase and planar hall effect in the skyrmion host Gd₂PdSi₃, *Phys. Rev. B* **101**, 220401(R) (2020).
- [7] M. Hirschberger, L. Spitz, T. Nomoto, T. Kurumaji, S. Gao, J. Masell, T. Nakajima, A. Kikkawa, Y. Yamasaki, H. Sagayama, H. Nakao, Y. Taguchi, R. Arita, T. H. Arima, and Y. Tokura, Topological Nernst effect of the two-dimensional skyrmion lattice, *Phys. Rev. Lett.* **125**, 076602 (2020).
- [8] H. Zhang, Q. Huang, L. Hao, J. Yang, K. Noordhoek, S. Pandey, H. Zhou, and J. Liu, Anomalous magnetoresistance in centrosymmetric skyrmion-lattice magnet Gd₂PdSi₃, *New J. Phys.* **22**, 083056 (2020).
- [9] S. Spachmann, A. Elghandour, M. Frontzek, W. Löser, and R. Klingeler, Magnetoelastic coupling and phases in the skyrmion lattice magnet Gd₂PdSi₃ discovered by high-resolution dilatometry, *Phys. Rev. B* **103**, 184424 (2021).
- [10] J. Ju, H. Saito, T. Kurumaji, M. Hirschberger, A. Kikkawa, Y. Taguchi, T. H. Arima, Y. Tokura, and T. Nakajima, Polarized neutron scattering study of the centrosymmetric skyrmion host material Gd₂PdSi₃, *Phys. Rev. B* **107**, 024405 (2023).
- [11] K. K. Kolincio, M. Hirschberger, J. Masell, T. H. Arima, N. Nagaosa, and Y. Tokura, Kagome lattice promotes chiral spin fluctuations, *Phys. Rev. Lett.* **130**, 136701 (2023).
- [12] M. Hirschberger, T. Nakajima, S. Gao, L. Peng, A. Kikkawa, T. Kurumaji, M. Kriener, Y. Yamasaki, H. Sagayama, H. Nakao, *et al.*, Skyrmion phase and competing magnetic orders on a breathing kagomé lattice, *Nat. Commun.* **10**, 5831 (2019).
- [13] M. Hirschberger, S. Hayami, and Y. Tokura, Nanometric skyrmion lattice from anisotropic exchange interactions in a centrosymmetric host, *New J. Phys.* **23**, 023039 (2021).
- [14] M. O. Ogunbunmi, H. S. Nair, and A. M. Strydom, Magnetic frustration-driven ground state properties of rare-earth magnetic ions on a breathing kagome lattice: a review of the Gd₃Ru₄Al₁₂ structure type magnets, *Crit. Rev. Solid State Mater. Sci.* **48**, 480 (2023).
- [15] N. D. Khanh, T. Nakajima, X. Yu, S. Gao, K. Shibata, M. Hirschberger, Y. Yamasaki, H. Sagayama, H. Nakao, L. Peng, *et al.*, Nanometric square skyrmion lattice in a centrosymmetric tetragonal magnet, *Nat. Nanotechnol.* **15**, 444 (2020).
- [16] Y. Yasui, C. J. Butler, N. D. Khanh, S. Hayami, T. Nomoto, T. Hanaguri, Y. Motome, R. Arita, T. H. Arima, Y. Tokura, *et al.*, Imaging the coupling between itinerant electrons and localised moments in the centrosymmetric skyrmion magnet GdRu₂Si₂, *Nat. Commun.* **11**, 5925 (2020).
- [17] N. D. Khanh, T. Nakajima, S. Hayami, S. Gao, Y. Yamasaki, H. Sagayama, H. Nakao, R. Takagi, Y. Motome, Y. Tokura, T. H. Arima, and S. Seki, Zoology of multiple-q spin textures in a centrosymmetric tetragonal magnet with itinerant electrons, *Adv. Sci.* **9**, 2105452 (2022).
- [18] N. Matsuyama, T. Nomura, S. Imajo, T. Nomoto, R. Arita, K. Sudo, M. Kimata, N. D. Khanh, R. Takagi, Y. Tokura, S. Seki, K. Kindo, and Y. Kohama, Quantum oscillations in the centrosymmetric skyrmion-hosting magnet GdRu₂Si₂, *Phys. Rev. B* **107**, 104421 (2023).

- (2023).
- [19] G. D. A. Wood, D. D. Khalyavin, D. A. Mayoh, J. Bouaziz, A. E. Hall, S. J. R. Holt, F. Orlandi, P. Manuel, S. Blügel, J. B. Staunton, O. A. Petrenko, M. R. Lees, and G. Balakrishnan, Double- q ground state with topological charge stripes in the centrosymmetric skyrmion candidate GdRu_2Si_2 , *Phys. Rev. B* **107**, L180402 (2023).
- [20] S. Eremeev, D. Glazkova, G. Poelchen, A. Kraiker, K. Ali, A. Tarasov, S. Schulz, K. Kliemt, E. Chulkov, V. Stolyarov, *et al.*, Insight into the electronic structure of the centrosymmetric skyrmion magnet GdRu_2Si_2 , *Nanoscale Adv.* **5**, 6678 (2023).
- [21] H. Yoshimochi, R. Takagi, J. Ju, N. Khanh, H. Saito, H. Sagayama, H. Nakao, S. Itoh, Y. Tokura, T. Arima, *et al.*, Multi-step topological transitions among meron and skyrmion crystals in a centrosymmetric magnet, arXiv preprint (2024), arXiv:2402.13751 [cond-mat.mtrl-sci].
- [22] R. Takagi, N. Matsuyama, V. Ukleev, L. Yu, J. S. White, S. Francoual, J. R. Mardegan, S. Hayami, H. Saito, K. Kaneko, *et al.*, Square and rhombic lattices of magnetic skyrmions in a centrosymmetric binary compound, *Nat. Commun.* **13**, 1472 (2022).
- [23] T. Shang, Y. Xu, D. J. Gawryluk, J. Z. Ma, T. Shiroka, M. Shi, and E. Pomjakushina, Anomalous hall resistivity and possible topological hall effect in the EuAl_4 antiferromagnet, *Phys. Rev. B* **103**, L020405 (2021).
- [24] X. Y. Zhu, H. Zhang, D. J. Gawryluk, Z. X. Zhen, B. C. Yu, S. L. Ju, W. Xie, D. M. Jiang, W. J. Cheng, Y. Xu, M. Shi, E. Pomjakushina, Q. F. Zhan, T. Shiroka, and T. Shang, Spin order and fluctuations in the EuAl_4 and EuGa_4 topological antiferromagnets: A μSR study, *Phys. Rev. B* **105**, 014423 (2022).
- [25] T. Okubo, S. Chung, and H. Kawamura, Multiple- q states and the skyrmion lattice of the triangular-lattice heisenberg antiferromagnet under magnetic fields, *Phys. Rev. Lett.* **108**, 017206 (2012).
- [26] A. Leonov and M. Mostovoy, Multiply periodic states and isolated skyrmions in an anisotropic frustrated magnet, *Nat. Commun.* **6**, 8275 (2015).
- [27] V. Lohani, C. Hickey, J. Masell, and A. Rosch, Quantum skyrmions in frustrated ferromagnets, *Phys. Rev. X* **9**, 041063 (2019).
- [28] J. Pang, X. Niu, H. J. Zhao, Y. Zhang, and L. Bellaiche, Unravelling spontaneous Bloch-type skyrmion in centrosymmetric two-dimensional magnets, arXiv preprint (2023), arXiv:2312.00423 [cond-mat.mtrl-sci].
- [29] J. Bouaziz, E. Mendive-Tapia, S. Blügel, and J. B. Staunton, Fermi-surface origin of skyrmion lattices in centrosymmetric rare-earth intermetallics, *Phys. Rev. Lett.* **128**, 157206 (2022).
- [30] J. A. M. Paddison, B. K. Rai, A. F. May, S. Calder, M. B. Stone, M. D. Frontzek, and A. D. Christianson, Magnetic interactions of the centrosymmetric skyrmion material Gd_2PdSi_3 , *Phys. Rev. Lett.* **129**, 137202 (2022).
- [31] R. Ozawa, S. Hayami, and Y. Motome, Zero-field skyrmions with a high topological number in itinerant magnets, *Phys. Rev. Lett.* **118**, 147205 (2017).
- [32] S. Hayami, R. Ozawa, and Y. Motome, Effective bilinear-biquadratic model for noncoplanar ordering in itinerant magnets, *Phys. Rev. B* **95**, 224424 (2017).
- [33] S. Hayami and Y. Motome, Square skyrmion crystal in centrosymmetric itinerant magnets, *Phys. Rev. B* **103**, 024439 (2021).
- [34] S. Hayami, Multiple skyrmion crystal phases by itinerant frustration in centrosymmetric tetragonal magnets, *J. Phys. Soc. Japan* **91**, 023705 (2022).
- [35] S. Hayami, Anisotropic skyrmion crystal on a centrosymmetric square lattice under an in-plane magnetic field, arXiv preprint (2023), arXiv:2312.01542 [cond-mat.str-el].
- [36] T. Nomoto, T. Koretsune, and R. Arita, Formation mechanism of the helical \mathbf{Q} structure in Gd-based skyrmion materials, *Phys. Rev. Lett.* **125**, 117204 (2020).
- [37] T. Nomoto and R. Arita, *Ab initio* exploration of short-pitch skyrmion materials: Role of orbital frustration, *J. Appl. Phys.* **133**, 150901 (2023).
- [38] N. Kanazawa, S. Seki, and Y. Tokura, Noncentrosymmetric magnets hosting magnetic skyrmions, *Adv. Mater.* **29**, 1603227 (2017).
- [39] M. Garst, J. Waizner, and D. Grundler, Collective spin excitations of helices and magnetic skyrmions: review and perspectives of magnonics in non-centrosymmetric magnets, *J. Phys. D: Appl. Phys.* **50**, 293002 (2017).
- [40] T. Weber, D. M. Fobes, J. Waizner, P. Steffens, G. S. Tucker, M. Böhm, L. Beddrich, C. Franz, H. Gabold, R. Bewley, *et al.*, Topological magnon band structure of emergent Landau levels in a skyrmion lattice, *Science* **375**, 1025 (2022).
- [41] M. Soda, E. M. Forgan, E. Blackburn, E. Campillo, V. Ryukhtin, I. Hoffmann, A. Kikkawa, Y. Taguchi, H. Yoshizawa, and H. Kawano-Furukawa, Asymmetric slow dynamics of the skyrmion lattice in MnSi , *Nat. Phys.* **19**, 1476 (2023).
- [42] S. J. Blundell, R. De Renzi, T. Lancaster, and F. L. Pratt, *Muon Spectroscopy: An Introduction* (Oxford University Press, Oxford, 2021).
- [43] K. J. A. Franke, B. M. Huddart, T. J. Hicken, F. Xiao, S. J. Blundell, F. L. Pratt, M. Crisanti, J. A. T. Barker, S. J. Clark, A. Štefančič, M. C. Hatnean, G. Balakrishnan, and T. Lancaster, Magnetic phases of skyrmion-hosting $\text{GaV}_4\text{S}_{8-y}\text{Se}_y$ ($y = 0, 2, 4, 8$) probed with muon spectroscopy, *Phys. Rev. B* **98**, 054428 (2018).
- [44] A. Štefančič, S. H. Moody, T. J. Hicken, M. T. Birch, G. Balakrishnan, S. A. Barnett, M. Crisanti, J. S. O. Evans, S. J. R. Holt, K. J. A. Franke, P. D. Hatton, B. M. Huddart, M. R. Lees, F. L. Pratt, C. C. Tang, M. N. Wilson, F. Xiao, and T. Lancaster, Origin of skyrmion lattice phase splitting in Zn-substituted Cu_2OSeO_3 , *Phys. Rev. Mater.* **2**, 111402(R) (2018).
- [45] T. J. Hicken, S. J. R. Holt, K. J. A. Franke, Z. Hawkhead, A. Štefančič, M. N. Wilson, M. Gomilšek, B. M. Huddart, S. J. Clark, M. R. Lees, F. L. Pratt, S. J. Blundell, G. Balakrishnan, and T. Lancaster, Magnetism and néel skyrmion dynamics in $\text{GaV}_4\text{S}_{8-y}\text{Se}_y$, *Phys. Rev. Res.* **2**, 032001(R) (2020).
- [46] T. J. Hicken, M. N. Wilson, K. J. A. Franke, B. M. Huddart, Z. Hawkhead, M. Gomilšek, S. J. Clark, F. L. Pratt, A. Štefančič, A. E. Hall, M. Ciomaga Hatnean, G. Balakrishnan, and T. Lancaster, Megahertz dynamics in skyrmion systems probed with muon-spin relaxation, *Phys. Rev. B* **103**, 024428 (2021).
- [47] M. N. Wilson, T. J. Hicken, M. Gomilšek, A. Štefančič, G. Balakrishnan, J. C. Loudon, A. C. Twitchett-Harrison, F. L. Pratt, M. Telling, and T. Lancaster, Spin dynamics in bulk MnNiGa and $\text{Mn}_{1.4}\text{Pt}_{0.9}\text{Pd}_{0.1}\text{Sn}$ investigated by muon spin relaxation, *Phys. Rev. B* **104**,

- 134414 (2021).
- [48] T. J. Hicken, M. N. Wilson, S. J. R. Holt, R. Khasanov, M. R. Lees, R. Gupta, D. Das, G. Balakrishnan, and T. Lancaster, Magnetism in the Néel-skyrmion host GaV_4S_8 under pressure, *Phys. Rev. B* **105**, 134414 (2022).
- [49] T. Hicken, M. Wilson, Z. Salman, T. Prokscha, A. Suter, F. Pratt, S. Zhang, G. van der Laan, T. Hesjedal, and T. Lancaster, Depth-dependent magnetic crossover in a room-temperature skyrmion-hosting multilayer, arXiv preprint (2022), [arXiv:2210.06070 \[cond-mat.str-el\]](https://arxiv.org/abs/2210.06070).
- [50] See Supplemental Material for details on crystal synthesis and characterization, AC susceptibility measurements, muon spectroscopy measurements, and *ab initio* (DFT) muon-site determination and analysis. This includes Refs. [1, 5–7, 29, 30, 42, 43, 51, 52, 57–61].
- [51] D. Beeman and P. Pincus, Nuclear Spin-Lattice Relaxation in Magnetic Insulators, *Phys. Rev.* **166**, 359 (1968).
- [52] N. Janša, A. Zorko, M. Gomilšek, M. Pregelj, K. W. Krämer, D. Biner, A. Biffin, C. Rüegg, and M. Klanjšek, Observation of two types of fractional excitation in the Kitaev honeycomb magnet, *Nat. Phys.* **14**, 786 (2018).
- [53] J. Jensen and A. R. Mackintosh, *Rare Earth Magnetism: Structures and Excitations* (Oxford University Press, 1991).
- [54] M. Mochizuki, Spin-wave modes and their intense excitation effects in skyrmion crystals, *Phys. Rev. Lett.* **108**, 017601 (2012).
- [55] X. Xing, Y. Zhou, and H. B. Braun, Magnetic skyrmion tubes as nonplanar magnonic waveguides, *Phys. Rev. Appl.* **13**, 034051 (2020).
- [56] P. Kotsanidis, J. Yakinthos, and E. Gamari-Seale, Magnetic properties of the ternary rare earth silicides $R_2\text{PdSi}_3$ ($R = \text{Pr, Nd, Gd, Tb, Dy, Ho, Er, Tm}$ and Y), *J. Magn. Magn. Mater.* **87**, 199 (1990).
- [57] F. Tang, M. Frontzek, J. Dshemuchadse, T. Leisegang, M. Zschornak, R. Mitrach, J.-U. Hoffmann, W. Löser, S. Gemming, D. C. Meyer, and M. Loewenhaupt, Crystallographic superstructure in $R_2\text{PdSi}_3$ compounds ($R = \text{heavy rare earth}$), *Phys. Rev. B* **84**, 104105 (2011).
- [58] B. Huddart, A. Hernández-Melián, T. Hicken, M. Gomilšek, Z. Hawkhead, S. Clark, F. Pratt, and T. Lancaster, Mufinder: A program to determine and analyse muon stopping sites, *Comput. Phys. Commun.* **280**, 108488 (2022).
- [59] S. J. Clark, M. D. Segall, C. J. Pickard, P. J. Hasnip, M. J. Probert, K. Refson, and M. Payne, First principles methods using CASTEP, *Z. Kristall.* **220**, 567 (2005).
- [60] J. P. Perdew, K. Burke, and M. Ernzerhof, Generalized gradient approximation made simple, *Phys. Rev. Lett.* **77**, 3865 (1996).
- [61] H. J. Monkhorst and J. D. Pack, Special points for Brillouin-zone integrations, *Phys. Rev. B* **13**, 5188 (1976).

Supplemental Material: Anisotropic Skyrmion and Multi- q Spin Dynamics in Centrosymmetric Gd_2PdSi_3

M. Gomilšek,^{1,2,3,*} T. J. Hicken,^{4,3} M. N. Wilson,^{5,3} K. J. A. Franke,^{6,3} B. M. Huddart,^{7,3} A. Štefančič,⁸ S. J. R. Holt,^{8,†} G. Balakrishnan,⁸ D. A. Mayoh,⁸ M. T. Birch,^{9,10,3} S. H. Moody,^{11,3} H. Luetkens,⁴ Z. Guguchia,⁴ M. T. F. Telling,¹² P. J. Baker,¹² S. J. Clark,³ and T. Lancaster³

¹*Jožef Stefan Institute, Jamova c. 39, SI-1000 Ljubljana, Slovenia*

²*Faculty of Mathematics and Physics, University of Ljubljana, Jadranska u. 19, SI-1000 Ljubljana, Slovenia*

³*Department of Physics, Durham University, South Road, Durham DH1 3LE, United Kingdom*

⁴*Laboratory for Muon Spin Spectroscopy, Paul Scherrer Institut, 5232 Villigen PSI, Switzerland*

⁵*Department of Physics and Physical Oceanography, Memorial University, A1B 3X7, Canada*

⁶*School of Physics and Astronomy, University of Leeds, LS2 9JT, United Kingdom*

⁷*Clarendon Laboratory, University of Oxford, Department of Physics, Oxford OX1 3PU, United Kingdom*

⁸*University of Warwick, Department of Physics, Coventry CV4 7AL, United Kingdom*

⁹*Max Planck Institute for Intelligent Systems, Heisenbergstrasse 3, D-70569 Stuttgart, Germany*

¹⁰*RIKEN Center for Emergent Matter Science, JP-351-0198 Wako, Japan*

¹¹*Laboratory for Neutron Scattering and Imaging, Paul Scherrer Institut, 5232 Villigen PSI, Switzerland*

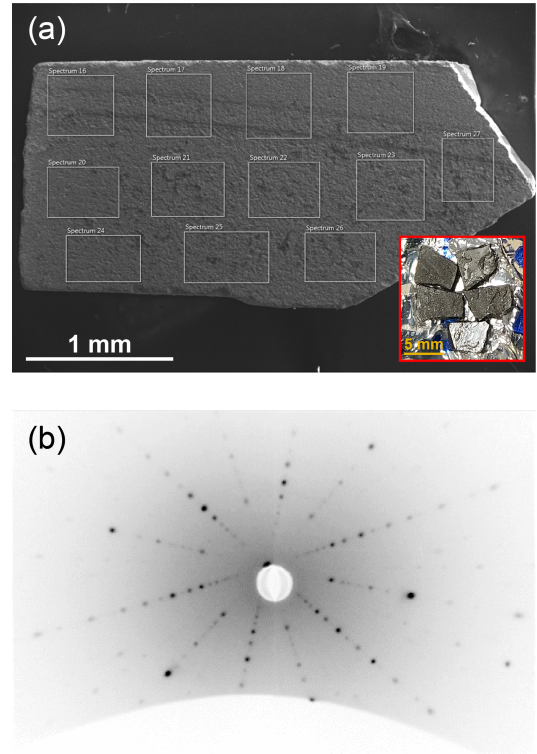
¹²*ISIS Facility, STFC Rutherford Appleton Laboratory, Didcot, Oxfordshire OX11 0QX, United Kingdom*

(Dated: March 14, 2024)

CRYSTAL SYNTHESIS, SEM-EDX, AND LAUE X-RAY MEASUREMENTS

Single-crystal sample synthesis was performed at the University of Warwick via the optical floating zone technique. Firstly, polycrystalline buttons of Gd_2PdSi_3 were synthesised by arc melting stoichiometric quantities of Gd (99.9%, STREM), Pd (99.9%, STREM), and Si (99.999%, Sigma-Aldrich). The buttons produced were flipped and remelted several times to ensure homogeneity. After the polycrystalline buttons were formed, they were recast into a rod for single-crystal growth. Single crystals of Gd_2PdSi_3 were then grown using a four-mirror optical image furnace (equipped with four xenon arc lamps). The crystals were grown in a high purity (6N) argon atmosphere. Crystal growth was carried out using a range of growth rates, from 8 to 12 mm/h, while the feed and seed rods were counter-rotated at speeds ranging from 10 to 20 rpm. This process yielded a single-crystal boule from which plate-like samples were extracted.

Compositional analysis was performed via scanning electron microscopy (SEM) with energy-dispersive X-ray (EDX) analysis on K_α edges of Gd, Pd, and Si on a Zeiss Supra 55-VP FEGSEM [Supplementary Fig. 1(a)]. The sample stoichiometry was measured to be $\text{Gd}_{2.04(3)}\text{Pd}_{1.05(1)}\text{Si}_3$, close to the ideal Gd_2PdSi_3 . Five plate-like, $\approx 9\text{ mm}^2 \times 0.6\text{ mm}$ samples were extracted from the single-crystal boule and polished for muon spectroscopy (μSR) and AC susceptibility measurements [inset in Supplementary Fig. 1(a)]. Sample orientation, with the crystallographic c axis perpendicular to the plates, was checked via Laue X-ray measurements, which found a maximal deviation from perfect alignment below 4° and good sample crystallinity [Supplementary Fig. 1(b)].



Supplementary Fig. 1. (a) SEM image of an extracted Gd_2PdSi_3 single-crystal sample with marked regions from which EDX spectra were analysed. Inset: mosaic of five Gd_2PdSi_3 samples in a silver foil packet for μSR measurements. (b) Laue pattern of an isolated single-crystal sample of Gd_2PdSi_3 .

AC SUSCEPTIBILITY MEASUREMENTS

Magnetic susceptibility with magnetic field $\mathbf{H} \parallel c$ and a drive field of 1 mT at 10 Hz was measured using a Quantum Design MPMS3 at the I10 support laboratory, Diamond Light Source. The single crystal sample was fixed to a quartz rod with GE varnish. The phase diagram [Fig. 1(a) in the main text] was determined using scans of increasing field from 0 to 2 T after zero field cooling (ZFC) the sample down from 30 K to each measured temperature.

MUON SPECTROSCOPY MEASUREMENTS

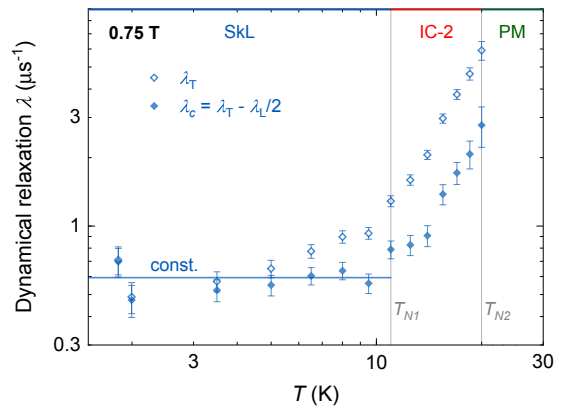
Plate-like samples were assembled in a mosaic before μ SR measurements [inset in Supplementary Fig. 1(a)]. Muon data from the GPS instrument at the Swiss Muon Source (S μ S) were fit using the Gaussian and exponential models described in the main text, since a damped-cosine-oscillation model [shown as a guide to the eye in Fig. 2(a) in the main text] proved unreliable since only the first minimum of the muon polarization could be clearly resolved at early times due to strong damping of the oscillatory contribution [Fig. 2(a) in the main text], due to the broadness of the quasi-static local-field distribution at the muon site, which made separating the oscillation frequency from the Gaussian damping coefficient hard. An alternative Kubo–Toyabe model [1], which describes muon polarization under a broad quasi-static local-field distribution in a powder or an isotropic magnetic system, was not appropriate as our samples were anisotropic single crystals.

Dynamical relaxation

At late times, exponential decay of muon polarization was observed [Fig. 2(a) in the main text]. In general, at late times, dynamical fluctuations of the local magnetic field $\mathbf{B}(t)$ at the muon site, which are described by the field–field autocorrelation function $\Phi_{\alpha\beta}(t) = 2\gamma_\mu^2 \langle \delta B_\alpha(t) \delta B_\beta(0) \rangle$ where $\delta \mathbf{B}(t) = \mathbf{B}(t) - \langle \mathbf{B} \rangle$, induce an exponential decay of muon polarization function along the detector direction, which we denote z , with a relaxation rate given by [1]

$$\lambda = \frac{1}{2} \int_0^\infty \cos(\omega_{0,z}t) [\Phi_{xx}(t) + \Phi_{yy}(t)], \quad (1)$$

where $\omega_{0,z} = \gamma_\mu \langle B_z \rangle$ is the Larmor angular frequency of the total magnetic field (applied plus internal) and $\gamma_\mu = 2\pi \times 135.53 \text{ MHz/T}$ is the muon gyromagnetic ratio. In other words, a component (z) of the muon spin relaxes at late times due to dynamical fluctuations of the local magnetic field in the plane perpendicular to that



Supplementary Fig. 2. Comparison of the raw TF muon relaxation rate (unfilled symbols) and the extracted relaxation rate due to out-of-plane (c -axis) spin fluctuations (solid symbols) in the SkL and IC-2 phases in a 0.75 T applied field.

component (xy -plane). If we have a crystal with uniaxial symmetry along the c axis, we thus have relaxation rates $\lambda_L = 2\lambda_{ab}$ and $\lambda_T = \lambda_{ab} + \lambda_c$, for muon spin components along $z = L \parallel c$ (LF) and $z = T \perp c$ (TF) directions, respectively, where the individual relaxation-rate contributions are

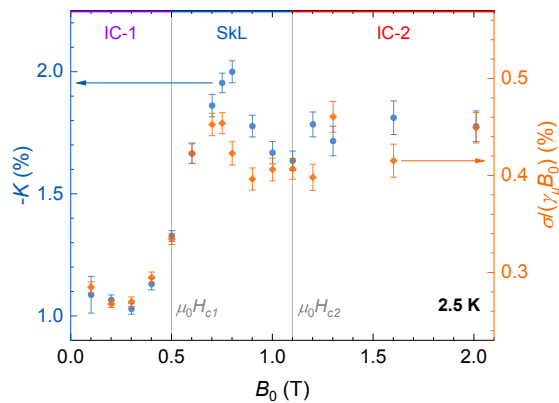
$$\begin{aligned} \lambda_{ab} &= \frac{1}{2} \int_0^\infty \cos(\omega_{0,z}t) \Phi_{aa}(t) = \lambda_L/2, \\ \lambda_c &= \frac{1}{2} \int_0^\infty \cos(\omega_{0,z}t) \Phi_{cc}(t) = \lambda_T - \lambda_L/2, \end{aligned} \quad (2)$$

and uniaxial symmetry ensures that $\Phi_{aa}(t) = \Phi_{bb}(t)$. Supplementary Fig. 2 shows the fitted TF relaxation rate λ_T and the out-of-plane relaxation-rate contribution λ_c extracted from it via Eq. (2). The latter is also shown on Fig. 3(a) in the main text. Where the temperatures at which λ_T and λ_L were measured did not match, λ_L was interpolated to the temperature of a given λ_T measurement before Eq. (2) was applied.

At low T , the dynamical relaxation rate under the spin-wave approximation for a single magnon band due to the two-magnon (Raman) process, which is expected the dominant one in relaxing the muon spin [2], is given by [2, 3]

$$\lambda \propto \int g^2(E) f(E) [1 + f(E)] dE \propto T^p e^{-\Delta/T}, \quad (3)$$

with $p = 2D/s - 1$ [Eq. (1) in the main text], where D is the dimensionality of spin-wave excitations with a spin density of states $g(E)$ at energy $E \propto \omega$, s is the dominant power in their dispersion relation $E - k_B \Delta \propto |\mathbf{q} - \mathbf{q}_0|^s$ around the ordering wave vector \mathbf{q}_0 , Δ is the magnon gap, $f(E) = 1/[\exp(\beta E) - 1]$ is the Bose–Einstein distribution function, $\beta = 1/(k_B T)$, and k_B is the Boltzmann constant. Note that Eq. (3) is formally only valid for $p > 0$ [3]. When the magnons are gapless ($\Delta = 0$) we recover power-law behaviour, $\lambda \propto T^p$, from the main text.



Supplementary Fig. 3. Field dependence of: the muon Knight shift (blue), and the quasi-static distribution width of local fields at the muon site normalized by the applied field (orange), at $T = 2.5$ K under TF. Vertical lines highlight critical fields.

Field dependence

We performed field-dependent TF μ SR measurements at a base $T = 2.5$ K on the HAL-9500 instrument at the μ S. In contrast to GPS measurements, the initial muon spin orientation pointed at an angle of $\theta \approx 90^\circ$ from the c axis [see Fig. 1(b) in the main text] to maximize the number of muon decays measured by TF detectors. Early-time data were fitted using a model consisting of a sum of two damped oscillations, $A(t) = a_s \cos(\omega t + \varphi) e^{-\sigma^2 t^2} + a_{\text{bgd}} \cos(\omega_0 t + \varphi_0)$, the first due to the sample, and the second due to the silver background. Here, the fitted silver-background angular frequency ω_0 gave an estimate of the applied magnetic field $B_0 = \omega_0 / \gamma_\mu$, whereas the fitted sample angular frequency ω yielded the local magnetic field $B = \omega / \gamma_\mu$ at the muon site. From these, the local muon Knight shift was calculated as $K = (B - B_0) / B_0 = \omega / \omega_0 - 1$ [1].

The obtained muon Knight shift is shown in [Supplementary Fig. 3](#), alongside the local field distribution width σ / γ_μ divided by the applied field B_0 . The obtained critical applied fields $\mu_0 H_{c1} = 0.5(1)$ T and $\mu_0 H_{c2} = 1.1(1)$ T are consistent with AC susceptibility [Fig. 1(a) in the main text] [4–6]. We see that in the IC-1 and IC-2 phases $K \propto \sigma / B_0 \approx \text{const.}$, which implies $B - B_0 \propto \sigma \propto B_0$ (i.e., the local average magnetization is proportional to the width of the magnetic field distribution, which is also approximately proportional to the applied magnetic field). On the other hand, $K \not\propto \sigma / B_0 \neq \text{const.}$ in the SkL phase, with both quantities showing clear peaks for applied fields near the middle of the phase. A similar peak in quasi-static magnetism is also observed in other SkL hosts near the middle of their SkL phases [7] (e.g., in noncentrosymmetric GaV_4S_8 and GaV_4Se_8 as a function of T). However, intriguingly, the peaks of K and σ / B_0 in Gd_2PdSi_3 appear to be slightly

shifted in field relative to each other, with the one in K appearing at $0.70(5)$ T and the one in σ / B_0 appearing at $0.80(5)$ T.

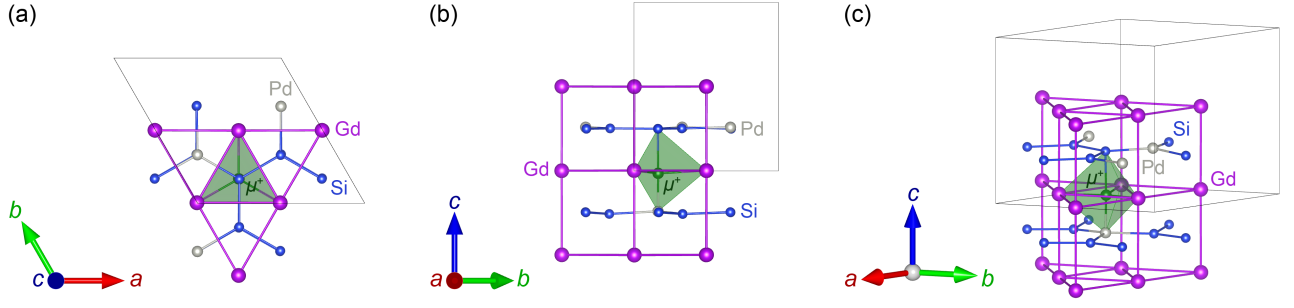
AB INITIO MUON SITE CALCULATIONS

Muon stopping sites were determined using the MuFinder program [8], which was used to run, cluster, and analyse the results of *ab initio* muon-stopping-site calculations performed using the CASTEP density functional theory (DFT) software [9]. For these, we used the PBE exchange–correlation functional [10] and ultra-soft pseudopotentials. Gd_2PdSi_3 forms a centrosymmetric superstructure with ABCDBADC stacking of inter-layer Pd and Si atomic configurations [4, 11]. Muon sites were calculated in a reduced superstructure with just two Pd/Si layers in the two most common layer stackings: AB and CD, as these two stackings already account for 50% of pairwise Pd/Si layer combinations in the full superstructure. The reduced unit cell dimensions of $8.16 \times 8.16 \times 8.19 \text{ \AA}^3$ were still large enough to avoid finite-size effects around the implanted muon. A 490 eV plane-wave energy cutoff and $2 \times 2 \times 2$ Monkhorst–Pack grid [12] reciprocal-space sampling was chosen to achieve DFT convergence. Total energies were converged to within 10^{-5} eV/atom in the self-consistent field (SCF) DFT loop, while muon-site geometry was converged to within a maximum force tolerance of 0.05 eV/\AA on both the muon and the nuclei.

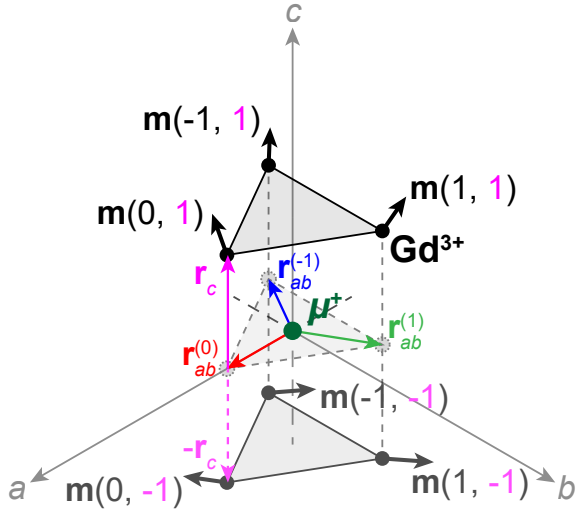
In all of the considered local stacking configurations, muons were found to occupy the same symmetric position at the centre of an *ab*-plane Gd^{3+} triangle ([Supplementary Fig. 4](#)), with only a small displacement of -0.29 and $+0.14 \text{ \AA}$ along the out-of-plane (c -axis) direction under AB and CD Pd/Si layer stacking, respectively. Due to the similarity between the stackings, we expect that all Gd^{3+} layers in Gd_2PdSi_3 host a muon site of this kind.

DIRECTIONS OF MAGNETIC FIELDS AT THE MUON SITE

To a good approximation, in- and out-of-plane components (\mathbf{m}_{ab} and \mathbf{m}_c) of Gd^{3+} spins generate in- and out-of-plane local magnetic fields ($\mathbf{B} \perp c$ and $\mathbf{B} \parallel c$) at this muon site, respectively. To see why this is so, we first observe that the claim is strictly true for: (i) effective contact hyperfine fields from all Gd^{3+} spins, and (ii) for dipolar fields from Gd^{3+} spins that lie in the same Gd layer as the muon, which includes the three dominant, nearest-neighbouring (NN) Gd^{3+} spins found at a distance $r_0 = 2.35 \text{ \AA}$ from the muon. This leaves only dipolar magnetic fields from Gd^{3+} spins on other layers than the muon, which could contribute in-plane magnetic fields due to out-of-plane Gd^{3+} spin components



Supplementary Fig. 4. Lowest-energy muon (μ^+) stopping site in Gd_2PdSi_3 (green). Shown are two neighbouring hexagonal Pd/Si (gray/blue, respectively) superstructure layers C and D around a triangular ab plane of Gd^{3+} ions (purple) in which the muon stops.



Supplementary Fig. 5. Geometry of the muon site from [Supplementary Fig. 4](#) showing the magnetic moments \mathbf{m} of the six Gd^{3+} spins discussed below.

and vice versa (we call these direction-mixing contributions to the local magnetic field). However, the closest Gd^{3+} spins on a separate layer from the muon are next-next-nearest-neighbouring (NNNN) ones, found at a distance $r' = 4.83 \text{ \AA}$ from the muon, that can contribute at most $(r_0/r')^3 = 12\%$ as much to the local magnetic field as the dominant, NN Gd^{3+} spins found in the same layer as the muon.

But the symmetric nature of the muon site further significantly reduces any direction-mixing contributions to the local magnetic field. Namely, in terms of positions of Gd^{3+} ions only, the muon site sits both on a mirror plane ab and on an axis of threefold symmetry perpendicular to that plane (i.e., along the c axis), with both filtering some of the direction-mixing contributions. Let us fix some notation. Any Gd^{3+} spin in Gd_2PdSi_3 displaced

by $\mathbf{r}_{ab}^{(0)}$ within the ab plane and by \mathbf{r}_c along the c axis [i.e., at $\mathbf{r}(0, 1) = \mathbf{r}_{ab}^{(0)} + \mathbf{r}_c$] from the muon, and possessing a magnetic moment $\mathbf{m}(0, 1)$, thus has ([Supplementary Fig. 5](#)): (i) a partner spin at $\mathbf{r}(0, -1) = \mathbf{r}_{ab}^{(0)} - \mathbf{r}_c$ with magnetic moment $\mathbf{m}(0, -1)$ under the approximate mirror-plane symmetry, and (ii) both of those have partner spins with magnetic moments $\mathbf{m}(j, \pm 1)$ at positions $\mathbf{r}(j, \pm 1) = \mathbf{r}_{ab}^{(j)} \pm \mathbf{r}_c$, where $\mathbf{r}_{ab}^{(j)} = R^j \mathbf{r}_{ab}^{(0)}$ for $j = -1, 0, 1$ and R_j is a rotation matrix for a rotation about the $+c$ axis by an angle of 120° , under the approximate threefold symmetry. Now, writing the dipolar contribution to the magnetic field of a magnetic moment \mathbf{m} at position \mathbf{r} as

$$\mathbf{B} = \frac{\mu_0}{4\pi r^3} \left(\frac{3}{r^2} [\mathbf{r} \otimes \mathbf{r}] \mathbf{m} - \mathbf{m} \right), \quad (4)$$

where μ_0 is the vacuum permeability, $r = |\mathbf{r}|$, and \otimes is the Kronecker product, we see that only the first term can mix directions. Written out for $\mathbf{r} = \mathbf{r}_{ab}^{(j)} \pm \mathbf{r}_c$ we can see that it is proportional to

$$\mathbf{r} \otimes \mathbf{r} = [\mathbf{r}_{ab}^{(j)} \otimes \mathbf{r}_{ab}^{(j)} + \mathbf{r}_c \otimes \mathbf{r}_c] \pm [\mathbf{r}_{ab}^{(j)} \otimes \mathbf{r}_c + \mathbf{r}_c \otimes \mathbf{r}_{ab}^{(j)}], \quad (5)$$

where the first term preserves directions (i.e., in- and out-of-plane components of Gd^{3+} magnetic moment \mathbf{m} generate in- and out-of-plane magnetic fields) and only the second term can mix directions. However, this latter, direction-mixing, term vanishes in [Eq. \(4\)](#) when $\mathbf{m}(j, 1) = \mathbf{m}(j, -1)$, i.e., if the spins displaced from the muon by \mathbf{r}_c and $-\mathbf{r}_c$ are aligned in the same direction. This is actually expected to be the main magnetization component in Gd_2PdSi_3 , as previous studies found predominantly ferromagnetic correlations between nearest-neighbouring Gd layers [13, 14]. However, we note that as spins at $\pm \mathbf{r}_c$ are an even number of Gd layers apart (as muon lies within a Gd layer; see [Supplementary Fig. 5](#)) even antiferromagnetic nearest-neighbour Gd layer correlations would lead to $\mathbf{m}(j, 1) = \mathbf{m}(j, -1)$, i.e. to complete suppression of the only direction-mixing term [[Eq. \(5\)](#)]. Only intermediate-wavelength inter-layer correlations could produce a direction-mixing magnetic field

at the muon site. More precisely, we can decompose pairs of magnetic moments as

$$\mathbf{m}(j, \pm 1) = \mathbf{m}^S(j) \pm \mathbf{m}^A(j), \quad (6)$$

where $\mathbf{m}^S(j) = [\mathbf{m}(j, 1) + \mathbf{m}(j, -1)]/2$ is the symmetric and $\mathbf{m}^A(j) = [\mathbf{m}(j, 1) - \mathbf{m}(j, -1)]/2$ is the antisymmetric component, where, according to Eqs. (4) and (5), only the latter can lead to direction mixing, but is expected to be subdominant [13, 14], i.e., we expect $|\mathbf{m}^A(j)| \ll |\mathbf{m}^S(j)|$.

Having thus completed the analysis of the impact of approximate ab -mirror-plane symmetry at the muon site, we now consider the influence of the approximate threefold symmetry about the local c axis (Supplementary Fig. 5). Firstly, we separate symmetric and antisymmetric magnetic moments in Eq. (6) into an ab -plane moment-direction component $\mathbf{m}_{ab}^{S,A}(j) \perp c$ and a c -axis moment-direction component $\mathbf{m}_c^{S,A}(j) \parallel c$, with $\mathbf{m}^{S,A}(j) = \mathbf{m}_{ab}^{S,A}(j) + \mathbf{m}_c^{S,A}(j)$. Secondly, from these we define contributions with chirality $\chi = -1, 0, 1$ via

$$\begin{aligned} \hat{\mathbf{m}}_{ab}^{S,A}(\chi) &= \frac{1}{3} \sum_{j=-1}^1 R^{-j\chi} \mathbf{m}_{ab}^{S,A}(j), \\ \hat{\mathbf{m}}_c^{S,A}(\chi) &= \frac{1}{3} \sum_{j=-1}^1 \omega^{-j\chi} \mathbf{m}_c^{S,A}(j), \end{aligned} \quad (7)$$

where $\omega = e^{2\pi i/3}$ is the third root of unity, and we have $\hat{\mathbf{m}}_c^{S,A}(\chi)^\dagger = \hat{\mathbf{m}}_c^{S,A}(-\chi)$ since $\mathbf{m}_c^{S,A}(j)$ are real vectors. Inversely, we can recover the magnetic moments from these chiral contributions via

$$\begin{aligned} \mathbf{m}_{ab}^{S,A}(j) &= \sum_{\chi=-1}^1 R^{j\chi} \hat{\mathbf{m}}_{ab}^{S,A}(\chi), \\ \mathbf{m}_c^{S,A}(j) &= \sum_{\chi=-1}^1 \omega^{j\chi} \hat{\mathbf{m}}_c^{S,A}(\chi). \end{aligned} \quad (8)$$

Inserting these definitions into the Eqs. (4) and (5) we finally see that only: (i) the positive chirality antisymmetric in-plane $\hat{\mathbf{m}}_{ab}^A(1)$, and (ii) non-zero chirality antisymmetric out-of-plane $\hat{\mathbf{m}}_c^A(\pm 1)$ magnetic components are direction-mixing, whereas all the others are not, including achiral ($\chi = 0$) ones. However, since the modulation wave lengths of incommensurate spin structure in Gd_2PdSi_3 are $\lambda \approx 25 \text{ \AA}$ [4, 15], and thus much larger than the nearest-neighbour Gd^{3+} -ion spacing $d_{\text{Gd-Gd}} = 4.08 \text{ \AA} \ll \lambda$, we expect achiral (i.e., locally approximately-ferromagnetic) components to dominate [4, 11], which thus leads to further strong suppression of direction-mixing contributions to the local magnetic field at the muon site.

In summary, to a good approximation, in- and out-of-plane components of Gd^{3+} spins are indeed expected to generate only in- and out-of-plane local magnetic fields

at this muon site, respectively, without mixing of in-plane Gd^{3+} spins components into out-of-plane magnetic fields and vice versa, since only dipolar fields from the strongly-subdominant chiral antisymmetric $\hat{\mathbf{m}}_{ab}^A(1)$ and $\hat{\mathbf{m}}_c^A(\pm 1)$ components of the spin structure in Gd planes displaced from the muon by a non-zero \mathbf{r}_c (i.e., far away from the muon) lead to any direction-mixing. Specifically, for the direction-mixing spin-structure components we have justified the following sequence of estimates: $|\hat{\mathbf{m}}_{ab}^A(1)|, |\hat{\mathbf{m}}_c^A(\pm 1)| \ll |\hat{\mathbf{m}}_{ab}^A(0)|, |\hat{\mathbf{m}}_c^A(0)| \ll |\hat{\mathbf{m}}_{ab}^S(0)|, |\hat{\mathbf{m}}_c^S(0)|$ with further suppression due to the distance from the muon by a factor $(r_0/r')^3 \ll 1$, and the mixing contribution only appearing in one quarter of the combined terms of Eqs. (4) and (5) for dipolar magnetic fields at the muon site. We can thus safely neglect any direction-mixing contributions to local magnetic fields in the analysis presented in the main text.

* matjaz.gomilsek@ijs.si

† Current addresses: Faculty of Engineering and Physical Sciences, University of Southampton, Southampton SO17 1BJ, United Kingdom; Max Planck Institute for the Structure and Dynamics of Matter, Luruper Chaussee 149, 22761 Hamburg, Germany

- [1] S. J. Blundell, R. De Renzi, T. Lancaster, and F. L. Pratt, *Muon Spectroscopy: An Introduction* (Oxford University Press, Oxford, 2021).
- [2] D. Beeman and P. Pincus, Nuclear Spin-Lattice Relaxation in Magnetic Insulators, *Phys. Rev.* **166**, 359 (1968).
- [3] N. Janša, A. Zorko, M. Gomilšek, M. Pregelj, K. W. Krämer, D. Biner, A. Biffin, C. Rüegg, and M. Klanjšek, Observation of two types of fractional excitation in the Kitaev honeycomb magnet, *Nat. Phys.* **14**, 786 (2018).
- [4] T. Kurumaji, T. Nakajima, M. Hirschberger, A. Kikkawa, Y. Yamasaki, H. Sagayama, H. Nakao, Y. Taguchi, T. H. Arima, and Y. Tokura, Skyrmion lattice with a giant topological hall effect in a frustrated triangular-lattice magnet, *Science* **365**, 914 (2019).
- [5] M. Hirschberger, T. Nakajima, M. Kriener, T. Kurumaji, L. Spitz, S. Gao, A. Kikkawa, Y. Yamasaki, H. Sagayama, H. Nakao, S. Ohira-Kawamura, Y. Taguchi, T. H. Arima, and Y. Tokura, High-field depinned phase and planar hall effect in the skyrmion host Gd_2PdSi_3 , *Phys. Rev. B* **101**, 220401(R) (2020).
- [6] M. Hirschberger, L. Spitz, T. Nomoto, T. Kurumaji, S. Gao, J. Masell, T. Nakajima, A. Kikkawa, Y. Yamasaki, H. Sagayama, H. Nakao, Y. Taguchi, R. Arita, T. H. Arima, and Y. Tokura, Topological Nernst effect of the two-dimensional skyrmion lattice, *Phys. Rev. Lett.* **125**, 076602 (2020).
- [7] K. J. A. Franke, B. M. Huddart, T. J. Hicken, F. Xiao, S. J. Blundell, F. L. Pratt, M. Crisanti, J. A. T. Barker, S. J. Clark, A. Štefančič, M. C. Hatnean, G. Balakrishnan, and T. Lancaster, Magnetic phases of skyrmion-hosting $\text{GaV}_4\text{S}_{8-y}\text{Se}_y$ ($y = 0, 2, 4, 8$) probed with muon spectroscopy, *Phys. Rev. B* **98**, 054428 (2018).
- [8] B. Huddart, A. Hernández-Melián, T. Hicken, M. Gomilšek, Z. Hawkhead, S. Clark, F. Pratt, and

- T. Lancaster, Mufinder: A program to determine and analyse muon stopping sites, *Comput. Phys. Commun.* **280**, 108488 (2022).
- [9] S. J. Clark, M. D. Segall, C. J. Pickard, P. J. Hasnip, M. J. Probert, K. Refson, and M. Payne, First principles methods using CASTEP, *Z. Kristall.* **220**, 567 (2005).
- [10] J. P. Perdew, K. Burke, and M. Ernzerhof, Generalized gradient approximation made simple, *Phys. Rev. Lett.* **77**, 3865 (1996).
- [11] F. Tang, M. Frontzek, J. Dshemuchadse, T. Leisegang, M. Zschornak, R. Mitrach, J.-U. Hoffmann, W. Löser, S. Gemming, D. C. Meyer, and M. Loewenhaupt, Crystallographic superstructure in $R_2\text{PdSi}_3$ compounds (R = heavy rare earth), *Phys. Rev. B* **84**, 104105 (2011).
- [12] H. J. Monkhorst and J. D. Pack, Special points for Brillouin-zone integrations, *Phys. Rev. B* **13**, 5188 (1976).
- [13] J. Bouaziz, E. Mendive-Tapia, S. Blügel, and J. B. Staunton, Fermi-surface origin of skyrmion lattices in centrosymmetric rare-earth intermetallics, *Phys. Rev. Lett.* **128**, 157206 (2022).
- [14] J. A. M. Paddison, B. K. Rai, A. F. May, S. Calder, M. B. Stone, M. D. Frontzek, and A. D. Christianson, Magnetic interactions of the centrosymmetric skyrmion material Gd_2PdSi_3 , *Phys. Rev. Lett.* **129**, 137202 (2022).
- [15] S. Li, X. Wang, and T. Rasing, Magnetic skyrmions: Basic properties and potential applications, *Interdiscip. Mater.* **2**, 260 (2023).